Available online at www.sciencedirect.com
SCIENCE DIRECT
Journal of the European Ceramic Society 26 (2006) 2707–2717
www.elsevier.com/locate/jeurceramsoc

High temperature–pressure synthesis of Ti-doped tohdite and corundum from hydrous Al_2O_3–TiO_2 gel

C. Pan [a], P. Shen [a,*], W.L. Huang [b], S.L. Hwang [c], T.F. Yui [d], H.T. Chu [e]

[a] *Institute of Materials Science and Engineering, National Sun Yat-sen University, Kaohsiung 80424, Taiwan, ROC*
[b] *Department of Geosciences, National Taiwan University, Taipei, Taiwan, ROC*
[c] *Department of Materials Science and Engineering, National Dong Hwa University, Hualien, Taiwan, ROC*
[d] *Institute of Earth Sciences, Academia Sinica, Taipei, Taiwan, ROC*
[e] *Central Geological Survey, P.O. Box 968, Taipei, Taiwan, ROC*

Received 30 April 2005; received in revised form 21 July 2005; accepted 31 July 2005
Available online 23 September 2005

Abstract

Hydrous Al_2O_3–TiO_2 (78:22 in molar ratio) gel was fired at various *P–T* conditions using a piston-cylinder apparatus and identified by XRD, FTIR, optical microscopy and electron microscopy. Below 675 °C, the sample remained amorphous at ambient pressure, yet transformed at 1.5 kbar to Ti-doped tohdite, which is elongated along the crystallographic *c*-axis, with well-developed (0 0 0 1) base and {1 0 $\bar{1}$ 0} ledges. Tohdite has a significant water/hydroxy content and is therefore susceptible to pore coalescence parallel to the basal layer upon electron dosage. Tohdite also contains Ti^{4+} up to 3 at.%, which replaces Al^{3+} in tetrahedral and/or octahedral sites to form superstructures and defect microstructures. In contrast, a higher *T–P* condition (above 675 °C and 8 kbar) caused the formation of more stable Ti-doped corundum, which is hexagonal-rhombohedral in shape and in epitaxial association with rutile nuclei. Ti-doped tohdite and corundum shed light on a sol–gel route for their occurrence in peraluminous metamorphic rock. The nanoporous and nanodelaminated tohdite may have potential catalytic applications.

Keywords: Electron microscopy; Defects; Porosity; Al_2O_3; TiO_2; Tohdite

1. Introduction

Alumina hydrates, namely gibbsite, bayerite, nordstrandite, boehmite, diaspore and tohdite, are the main precursors of various alumina polymorphs including the α-form, i.e. corundum with the packing of oxygen anions in hexagonal close packed scheme.[1,2] (Refer to Ref. [2] for the structure and stability of aluminum hydroxides from the theoretical viewpoint.)

Tohdite is $Al_2O_3{\cdot}0.2H_2O$ with hexagonal crystal structure (space group $P6_3mc$) originally named for a synthetic product.[3] It can be hydrothermally synthesized in the corundum *T–P* stable region[4–6] and transforms to corundum via intermediate phases, i.e. κ′-Al_2O_3 and then κ-Al_2O_3.[7] Mineralizers were known to modify the shape of tohdite, e.g. hexagonal plates in the presence of aluminum fluoride[4] and needles in the presence of titanium sulfate.[6] Tohdite in the form of nano crystallites embedded in an amorphous structure, was synthesized by ultrasonic spray pyrolysis in the presence of water mist.[8] Recently, we reported the discovery of natural Ti-bearing tohdite as submicrometer-size inclusions in garnet from whiteschist of the Kokchetav ultrahigh-pressure terrane, Kazakhstan.[9]

Ti-doped corundum has superior mechanical, thermal, optical, electrical and chemical properties for wide applications as microelectronics, optoelectronic devices, lasing crystals[10] and protective coatings on various substrates.[11] The asterism (star effect) in gem-quality star sapphire has long been known to be corundum associated with Ti impurities forming twin variants of titania via a solid state precipitation process.[12] It is however not clear whether

* Corresponding author. Tel.: +886 7 5252000 4060; fax: +886 7 5254099.
E-mail address: pshen@mail.nsysu.edu.tw (P. Shen).

0955-2219/$ – see front matter © 2005 Elsevier Ltd. All rights reserved.
doi:10.1016/j.jeurceramsoc.2005.07.058

titania is genetically related to Ti-doped tohdite and/or corundum in a sol–gel process.

The motivation for the present synthesis of Ti-doped tohdite and corundum from hydrous Al_2O_3–TiO_2 gel at high temperature and pressure is three-fold. Firstly, to link crystalline alumina hydrates and alumina to paleosols and metamorphism of hydrous gel at crustal depths. Secondly, to clarify the catalytic effect, if any, of Ti ion and/or TiO_2 on the nucleation of Ti-doped tohdite or corundum. Thirdly, to characterize the morphology and defect microstructures of Ti-doped tohdite and corundum that are of concern to the science and technology of alumina hydrates and alumina.[13]

2. Experimental procedure

2.1. Materials

The (hydrothermal) high *T*–*P* experiments were carried out by first synthesizing a Al_2O_3–TiO_2 (78:22 in molar ratio or 82:18 in weight ratio) gel after the method of Montoya et al.[14] In this sol–gel route, acid co-hydrolysis of precursors, i.e. aluminum tri-sec-butoxide $Al(OBu^s)_3$(ATSB) and titanium(IV) tetrabutoxide $Ti(OBu^n)_4$(TTB), was conducted in isopropanol solvent. Aluminum and titanium alkoxides were dissolved in 300 ml of isopropanol at 25 °C. The mixture was maintained under vigorous stirring for 3 h, followed by the dropwise addition of water. Isopropanol and HNO_3 solution, with specific reactants, were used in order to obtain the following molar ratios: HNO_3/(ATSB + TTB) = 0.2; H_2O/(ATSB + TTB) = 20; ROH/(ATSB + TTB) = 75 where R denotes radical. Beyond the gelation point, the material was aged without agitation for 4 days, and heated in oven for 3 h (at a final temperature of 85.5 °C) to form wet gel with 18 wt.% TiO_2 in solid solution.

2.2. Methods

Experiments were further performed in a piston cylinder apparatus at various *T*–*P* conditions (500 °C and 1.5 kbar, 675 °C and 8.5 kbar, 800 °C and 9 kbar) for up to 72 h (cf. sample numbers in Table 1) using a 1/2-in. piston. The chosen *P*–*T* conditions fall into the range of amphibolite to granulite facies metamorphism. The furnace assembly was constructed from graphite, talc and pyrophyllite. The pulverized gel was sealed in gold capsules with or without 10 wt.% addition of H_2O and then subjected to high *T*–*P* conditions. The temperatures, measured with chromel-alumel thermocouples, were accurate to ±10 °C. The hydraulic pressure was measured using a Heise gauge. All runs were brought to 2 kbar above the desired experimental pressure at room temperature. Then the pressure was adjusted to the experimental pressure after raising the temperature to the experimental temperature. The reported pressure is nominal. The gel powder under high *T*–*P* and hydrothermal conditions was not sintered, i.e. it remained as a loose aggregate, ready for phase identification by powder X-ray diffraction (XRD) in the 2θ range of 10–70° using a D-5000 Siemens diffractometer with Cu Kα radiation at 40 kV and 30 mA.

FT-IR spectroscopy (BRUKER IFS 66 v/s, resolution <0.25 cm^{-1}, spot size 1.2× the current aperture diameter, SiC glowbar as black body emitter, frequency range 7500–370 cm^{-1}, operation vacuum <3 mbar inside the optics bench) was used to characterize OH bands of Ti-doped tohdite mixed with KBr. Optical microscopy under plane polarized light and scanning electron microscopy (SEM, using a JSM-6400 instrument coupled with energy-dispersive X-ray (EDX) operated at 20 kV with a collector receiving counts at 36° to the top surface of the specimen holder) were used to study the microstructure and composition of the phases. The point count EDX analyses were also performed at 15 kV with a sintered specimen as standard to ensure that the semi-quantitative determination of the Ti or Al content in the phases is accurate within ±1 at.%. Analytical electron microscopy (AEM, JEOL3010 instrument operating at 300 kV) coupled with point-count EDX analysis at a beam size of 10–15 nm were used to determine local composition. The EDX analysis was performed using K shell counts for Al, Ti and O, and the ratio method without absorption correction.[15] Transmission electron microscopy (TEM) was used to take bright field image, dark field image and selected area electron diffraction (SAED) patterns for the identification of crys-

Table 1
High *T*–*P* experimental results of hydrous Al_2O_3–TiO_2 gel determined by XRD

Sample	*T* (°C)	*P* (kbar)	*t* (h)	H_2O[a]	Phases in the order of increasing content
#1	500	1.5	40	Yes	Anatase, rutile, tohdite
#2	500	1.5	40	No	Anatase, rutile, tohdite
#3	675	8.5	72	Yes	Rutile, β-Al_2O_3, α-Al_2O_3
#4	675	8.5	72	No	Rutile, β-Al_2O_3, α-Al_2O_3
#5	800	9	72	Yes	Rutile, α-Al_2O_3
#6	800	9	72	No	Rutile, α-Al_2O_3
#7	800	Ambient	12	No	Rutile, δ-Al_2O_3
#8	500	1.5	2	Yes	Rutile, anatase, nordstrandite, tohdite, χ-Al_2O_3, boehmite
#9	500	1.5	2	No	Boehmite, rutile, nordstrandite, χ-Al_2O_3, tohdite, anatase
#10	675	8.5	1	Yes	Nordstrandite, χ-Al_2O_3, tohdite, rutile, anatase
#11	675	8.5	1	No	Nordstrandite, χ-Al_2O_3, tohdite, rutile

[a] Optional 10 wt.% H_2O dilution.

talline phases and their defect microstructures. The sample grains are generally too thick to allow for conventional thin-film diffraction contrast. Nevertheless, the structure, shape and epitaxial crystallographic relationship of the crystalline phases, which are the foci of this study, were unambiguously determined by TEM. The thin areas at the corners and edges of the tohdite grains also gave valuable information of their cracking/coalescence behavior.

3. Results

3.1. XRD

XRD indicated that the sample remained amorphous up to 500 and 675 °C, but transformed to rutile, and δ-Al_2O_3 (JCPDS file 46-1131) when fired at 800 °C under ambient pressure (not shown). This is consistent with the previous DTA report that the sol–gel Al_2O_3–TiO_2 remains amorphous up to ca. 780 °C under ambient pressure.[14] (The typical DTA results gave an exothermic peak i.e. crystallization event at 840 °C for the sample with 86 wt.% Al_2O_3 and 14 wt.% TiO_2, and 782 °C for the sample with 56 wt.% Al_2O_3 and 44 wt.% TiO_2.[14])

Under high *P–T* conditions, however, the hydrous gels transformed to crystalline aluminum hydrates, alumina and titania with or without 10 wt.% H_2O dilution, as indicated by XRD traces in Fig. 1. The specific phases obtained in the order of increasing content were compiled in Table 1. Occasionally contamination by the Au capsule was shown by the XRD peaks of Au (JCPDS file 04-0784) and Au_2O_3 (JCPDS file 43-1039). In general, water dilution of the hydrous gel had little effect on the phase assemblages for a long experimental time at high *P–T* conditions (i.e. samples #1–#7 in Fig. 1a), but facilitated significantly the crystallization of aluminum hydrates for a short experimental time at relatively low *P–T* condition (i.e. samples #8–#11 in Fig. 1b) as addressed respectively in the following.

Anatase, rutile and tohdite were found for the sample fired at 1.5 kbar and 500 °C for 40 h regardless of H_2O dilution (Fig. 1a). Tohdite has a hexagonal structure with lattice parameters similar to those that were hydrothermally synthesized at 0.8–1.5 katm and 480–520 °C in the presence of mineralizer (JCPDS file 22-1119, $a = 0.5575$ nm, $c = 0.8761$ nm and $c/a = 1.571$).[6] The d-spacings and structure refinement indicated that tohdite has $a = 0.5571$ nm and $c = 0.8759$ nm when synthesized from hydrous gel, and $a = 0.5584$ nm and $c = 0.8788$ nm when synthesized with extra H_2O. In both cases, there is the additional effect of Ti dissolution on the cell parameters as discussed later. The samples fired at 8.5 kbar and 675 °C for 72 h contain rutile, β-Al_2O_3 and α-Al_2O_3 regardless of H_2O dilution in the synthesis (Fig. 1a). The identification of β-Al_2O_3 and α-Al_2O_3 was based on the relative intensity of the two peaks at 0.140 and 0.137 nm, the former being stronger for β-Al_2O_3 but weaker for α-Al_2O_3. (The relative intensity I/I_1 of the two peaks is 100:50 for β-Al_2O_3 (JCPDS file 10-0414), but 30:50 for α-Al_2O_3 (JCPDS file 10-173).) The present α-Al_2O_3 has a smaller lattice parameter ($a = 0.4750$ nm, $c = 1.2980$ nm) and a larger c/a ratio ($c/a = 2.733$) than that of JCPDS file 10-173 ($a = 0.4758$ nm, $c = 1.2991$ nm, $c/a = 2.730$), indicating a significant Ti dissolution in a corundum structure. The samples fired at 9 kbar and 800 °C for 72 h contain rutile and α-Al_2O_3 regardless of H_2O dilution (Fig. 1a).

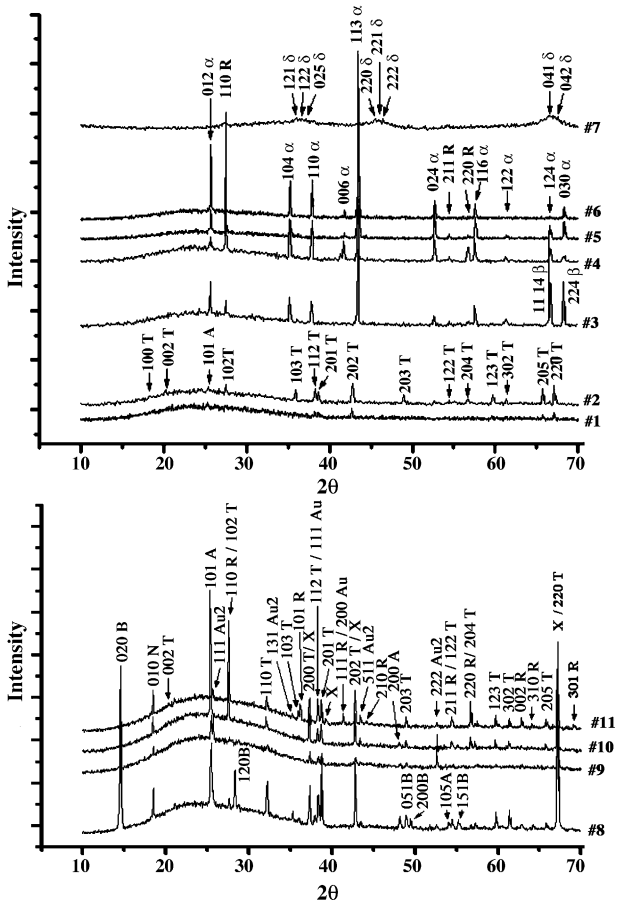

Fig. 1. X-ray diffraction (Cu Kα) traces of hydrous Al_2O_3–TiO_2 gel fired at various *T–P* and water dilution conditions specified in Table 1: (a) prolonged experiments for ≥12 h, samples #1–#7, (b) additional short experiments for ≤2 h, samples #8–#11. Notations: alumina (α-, β-, χ- and δ-type), tohdite (T), nordstrandite (N), boehmite (B), rutile (R), anatase (A). Gold (Au) and Au_2O_3(Au2) are due to contamination from capsule.

Additional experiments conducted for a short time at relatively low *P–T* conditions, i.e. 500 °C, 1.5 kbar for 2 h and 675 °C, 8.5 kbar for 1 h (Fig. 1b), showed that boehmite and/or nordstrandite transformed to tohdite and anatase changed to rutile. The identification of these and additional metastable aluminum hydrates and alumina was based on JCPDS files: boehmite (AlO(OH), JCPDS file21-1307), nordstrandite ($Al(OH)_3$, JCPDS file 24-0006), χ-Al_2O_3 (JCPDS file 34-0493). (According to Ref. [6] boehmite and even χ-Al_2O_3 can transform to tohdite under hydrothermal conditions.) It is noteworthy that the presence of additional H_2O in such synthesis conditions facilitated the crystal-

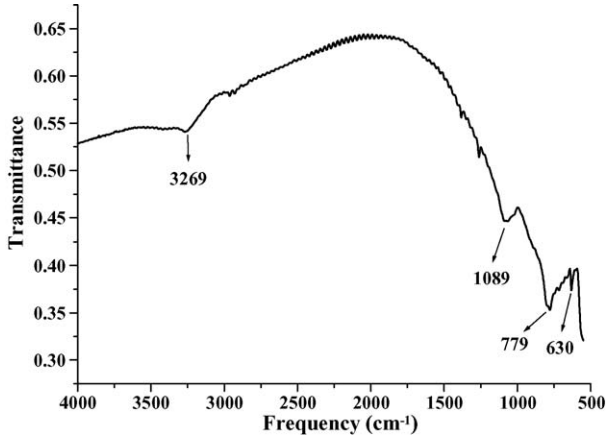

Fig. 2. FT-IR spectrum of Ti-containing tohdite in sample #2, showing bands at 3269 and 1089 cm^{-1} for the OH stretching and deformation modes, respectively. The Ti free tohdite synthesized at 1000 atm and 480 °C has bands at 3260 and 1140 cm^{-1} for the OH stretching and deformation modes, respectively.[5] A higher frequency for OH stretching, yet lower frequency for OH deformation in the present sample may be due to a higher synthesis pressure and/or Ti content. Extra absorption at 779 and 630 cm^{-1} can be attributed to Al-doped anatase having slightly higher wave numbers than undoped anatase, i.e. 739 and 611 cm^{-1}, respectively.[17]

lization and polymorphic change of both aluminum hydrate and titania in the incipient stage.

3.2. FT-IR spectrum

Ti-dissolved tohdite synthesized at 1.5 kbar and 500 °C for 40 h without additional H_2O showed IR bands at 3269 and 1089 cm^{-1} for the OH stretching and deformation modes, respectively (Fig. 2). The Ti-free tohdite synthesized at 1000 atm and 480 °C showed bands at 3260 and 1140 cm^{-1} for the OH stretching and deformation modes, respectively.[5] The OH deformation band can be assigned to a bulk OH group[16] whereas the broad OH stretching band with a relatively high wave number, i.e. above 3260 cm^{-1}, can be attributed to water molecules analogous to the assignment (near 3400 cm^{-1}) for poorly crystalline boehmite.[16] A higher frequency for OH stretching, yet lower frequency for OH deformation in the present sample, may be due to a higher synthesis pressure (1.5 kbar) and/or the Ti dissolution. Additional absorption at 779 and 630 cm^{-1} can be attributed to Al-doped anatase having slightly higher wave numbers than undoped anatase, i.e. 739 and 611 cm^{-1}, respectively.[17]

3.3. Optical polarized microscopy

Fig. 3a shows the representative optical micrograph of rod-like tohdite formed under 500 °C and 1.5 kbar for 2 h with

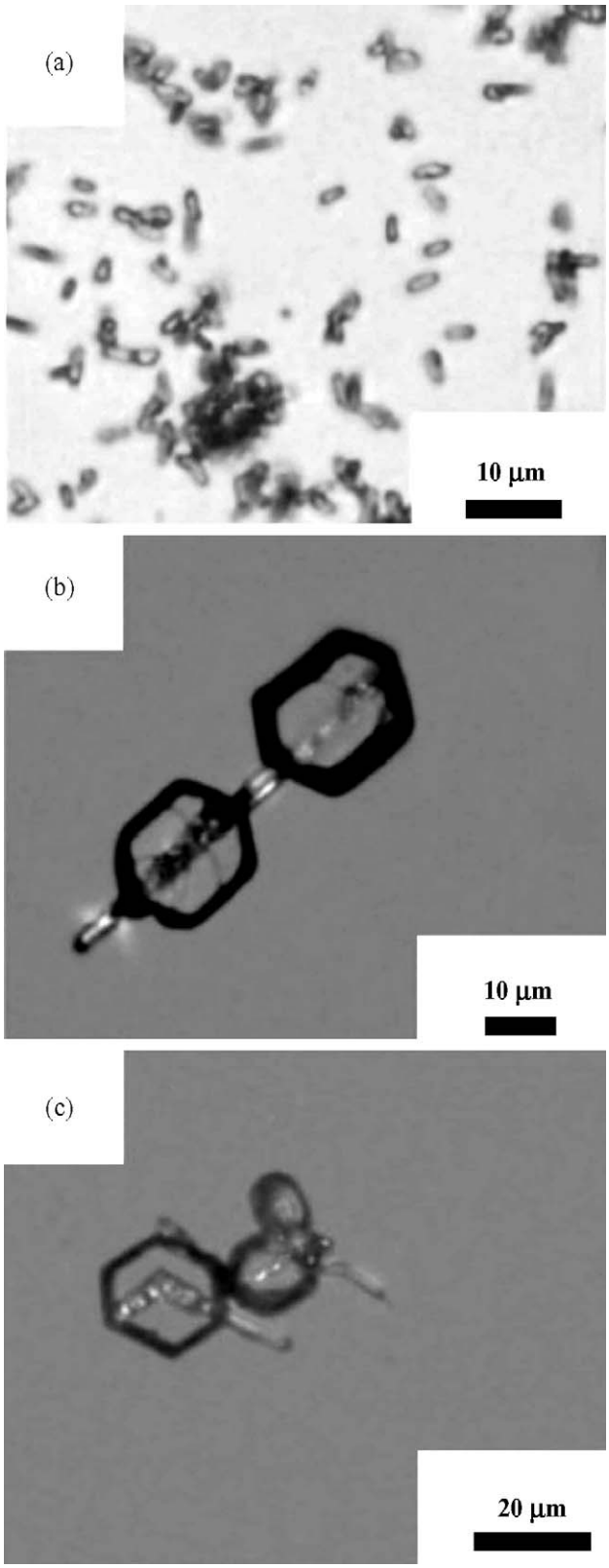

Fig. 3. Optical micrographs of crystalline aluminum hydrate/alumina and titania formed under specified *P–T* conditions: (a) rod-like tohdite in sample #8, (b) rod-like rutile in epitaxial association with hexagonal corundum in sample #5, (c) geniculated twin of rutile in epitaxial association with hexagonal corundum in sample #6. Panel (a) was taken under open polarizer, whereas panels (b) and (c) under crossed polarizers with additional λ plate to show otherwise unrecognized corundum in extinction orientation.

10 wt.% H_2O addition. The high relief under open polarizer (Fig. 3a) and low birefringence under crossed polarizers (not shown) are in accord with the reported refractive indices $\omega = 1.738–1.748$, $\omega - \varepsilon < 0.01$.[4] The rod-like rutiles with a high birefringence, length-slow and parallel extinction were found to be in association with hexagonal corundum as viewed in extinction orientation under crossed polarizers for the sample fired at 800 °C and 9 kbar for 72 h in the presence of additional 10 wt.% H_2O (Fig. 3b). Geniculate twins of rutile and hexagonal-rhombohedral α-Al_2O_3 were also observed for the sample fired at 675 °C and 8.5 kbar for 72 h unaffected by the absence of H_2O (Fig. 3c). The sample fired at 800 °C under ambient pressure contained δ-Al_2O_3 and rutile according to XRD. Gel devitrification of this sample was indeed manifested by interference color; however, the individual crystallites were too small to be resolved by optical microscopy (not shown).

3.4. SEM

SEM image of the samples fired at 500 °C/1.5 kbar for 40 h without the addition of H_2O (Fig. 4a) indicated that tohdite typically formed rugby-like rods ca. 1 μm in width and 5 μm in length. The samples fired at 675 °C/8.5 kbar for 40 h (Fig. 4b) and 800 °C/9.0 kbar for 72 h (Fig. 4c) typically showed hexagonal-rhombohedral α-Al_2O_3 ca. 2∼50 μm in size, which were penetrated by rutile in the form of rods or geniculate twins. There are ca. 2 ± 1 at.% Ti in tohdite and α-Al_2O_3 and ca.3 ± 1 at.% Al in rutile according to point-count EDX analysis (not shown), consistent with the AEM analysis addressed later.

3.5. TEM

The SAED pattern of tohdite in the [1 $\bar{1}$ 0 0] zone axis originally showed no extra spots (Fig. 5a). A tohdite rod is always elongated along its crystallographic c-axis and has a well-developed (0 0 0 1) face and {1 0 $\bar{1}$ 0} faces as shown by BFI of the examples in end-on view (Fig. 5b) and side view in the [$\bar{1}$ 2 $\bar{1}$ 0] zone axis (Fig. 5c). Upon electron irradiation, the tohdite (1 0 $\bar{1}$ 0) diffraction became dimmed in the [$\bar{1}$ 2 $\bar{1}$ 0] zone axis (Fig. 5d), which can be attributed to the epitaxial dehydration product of tohdite, i.e. κ-Al_2O_3 ($a = 0.469$ nm, $b = 0.818$ nm, $c = 0.887$ nm, space group $Pna2_1$,[18,19]) following specific crystallographic relationship to tohdite (denoted as t): $[\bar{1}\,2\,\bar{1}\,0]_t // [0\,1\,0]_\kappa$; $(0\,0\,0\,1)_t // (0\,0\,1)_\kappa$.

The tohdite rods showed growth ledges (Fig. 6a) and pores (Fig. 6b) and microcracks parallel to the basal layers (Fig. 6c) as represented by the sample fired at 500 °C and 1.5 kbar for 40 h with additional 10 wt.% H_2O. The nano and microcracks tended to coalesce to form large cracks with resultant delaminated nanosheets parallel to the basal layer upon electron irradiation for minutes (Fig. 6d). This cracking/coalescence behavior is analogous to the dehydroxylation of interstratified phyllosilicates[20] or the dehydration of gibbsite to form pores and χ-Al_2O_3.[21] The well-developed microcracks along the basal layers and the growth ledges at lateral faces (1 0 $\bar{1}$ 0) can be accounted for by the enrichment of OH^- and/or H_2O along the (0 0 0 1) and (1 0 $\bar{1}$ 0) planes (cf. Appendix A).

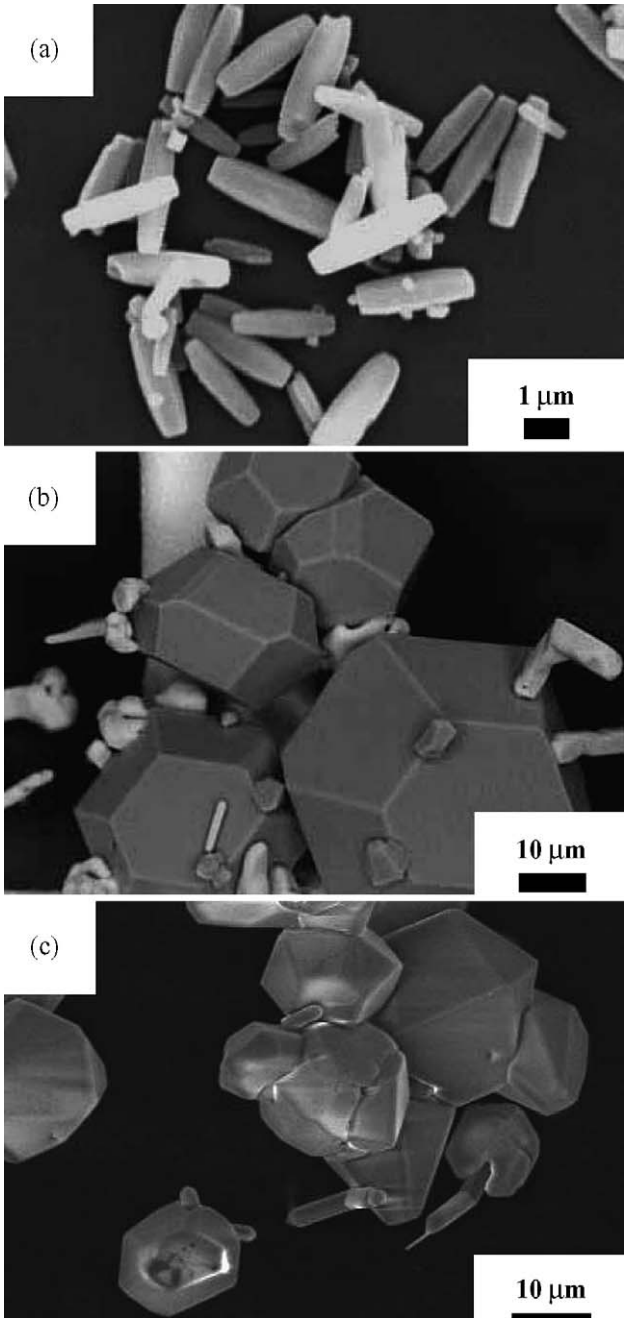

Fig. 4. SEM micrographs of crystalline aluminum hydrate/alumina and titania formed under specified *P–T* conditions: (a) SEI of rod-like tohdite ca. 1 μm in width and 5 μm in length in sample #2, (b) BEI of rod-like and geniculate twinned rutile and hexagonal-rhombohedral corundum in sample #4, and (c) SEI of geniculate twinned rutile and hexagonal-rhombohedral corundum in sample #6.

The α-Al_2O_3 typically formed hexagonal-rhombohedra with well-developed ($\bar{1}\,\bar{1}\,2\,0$), ($0\,\bar{1}\,1\,\bar{2}$) and ($\bar{1}\,0\,1\,2$) faces as shown edge-on in the [$2\,\bar{2}\,0\,1$] zone axis (Fig. 7a) for the representative sample fired at 675 °C and 8.5 kbar for

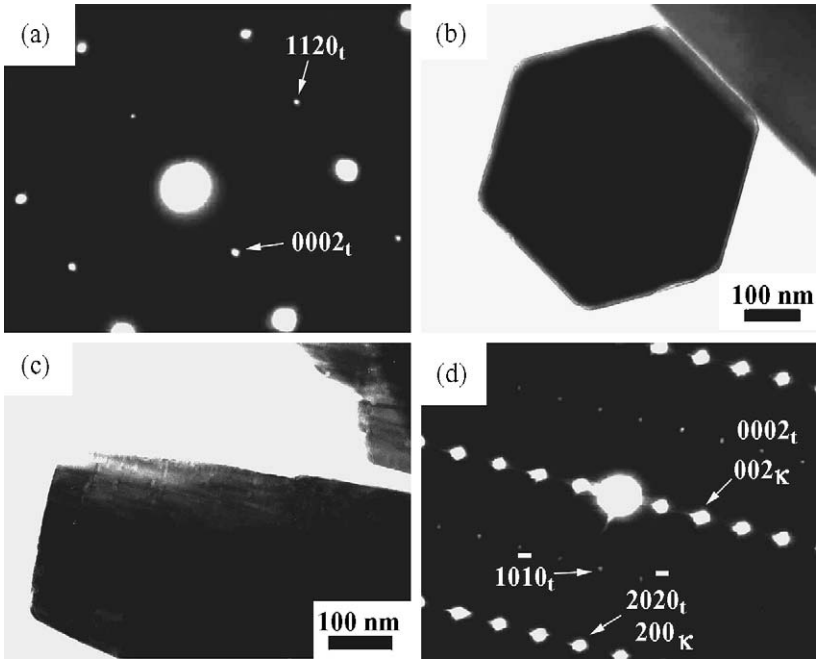

Fig. 5. TEM of tohdite in sample #2. (a) SAED pattern of tohdite in $[1\,\bar{1}\,0\,0]$ zone axis. (b and c) BFIs of tohdite in end-on ([0 0 0 1] zone axis) and side view ($[\bar{1}\,2\,\bar{1}\,0]$ zone axis) orientation, respectively. (d) SAED pattern of tohdite (denoted as t) in the $[\bar{1}\,2\,\bar{1}\,0]$ zone axis upon electron irradiation to form κ-Al_2O_3 (denoted as κ) following specific crystallographic relationship: $[\bar{1}\,2\,\bar{1}\,0]_t//[0\,1\,0]_\kappa$; $(0\,0\,0\,1)_t//(0\,0\,1)_\kappa$. Note $(0\,0\,1)_\kappa$ and $(0\,0\,0\,1)_t$ are double diffractions according to the space group selection rule of $Pna2_1$ and $P6_3mc$, respectively.

72 h with 10 wt.% H_2O. These faces are all about the Wulff shape of crystal due to a beneficial lower (h k l)-specific surface energy.[22] Geniculated twins of rutile and corundum, as revealed by optical microscopy under plane polarized light in Fig. 3c, were further characterized by TEM BFI and SAED pattern to follow a specific crystallographic relationship, i.e. $[0\,0\,1]_R//[0\,0\,0\,1]_\alpha$; $(0\,\bar{1}\,1)_R//(1\,\bar{2}\,1\,0)_\alpha$ (Fig. 7b).

Point count EDX analysis indicated that tohdite has ca. 3 at.% Ti in solid solution as represented by the sample fired at 500 °C and 1.5 kbar for 40 h without additional H_2O (Fig. 8a). Previous determination by the colorimetric analysis method for the samples synthesized at 480–520 °C and 800–1500 atm gave similar results.[6] α-Al_2O_3has ca, 2 at.% Ti in solid solution as indicated by the sample fired at 675 °C and 8.5 kbar for 72 h with additional 10 wt.% H_2O (Fig. 8b). Rutile, which is stable at 800 °C and 9.0 kbar, was found to contain ca. 2 at.% Al (Fig. 8c).

4. Discussion

4.1. Catalytic nuclei and energetics for tohdite and corundum

It is unclear whether or not the tohdite formation in the hydrous Al_2O_3–TiO_2 gel is a nucleation and growth process, an ordering reaction or some form of spinodal decomposition. In any case, a hydrous sol–gel component is essential for the present formation of tohdite. Theoretically, Mathieu et al.[28] declared that there is no temperature range for aluminum hydroxide to form tohdite. Their theory accounts for difficulty of tohdite production by simple dehydration of aluminum hydroxide at a low water vapor pressure. Only under conditions of hydrothermal synthesis tohdite may be formed. It is also noteworthy that the structure of tohdite is the only one (among aluminum hydrates) in which simple hydrogen jumps are not sufficient to generate internal water molecules. Hydrogen atoms have to diffuse into the structure to form H_2O groups, which tend to be removed upon calcination.[28]

Tohdite formation has nothing to do with crystalline titania, yet may possibly be catalyzed by Ti^{4+}, because of its coordination and polymerization effects in the Al_2O_3–SiO_2–ZnO melts[23,24] or gel.[25] Tohdite in the form of nano crystallites embedded in an amorphous structure, was synthesized by ultrasonic spray pyrolysis in the presence of water mist.[8] This implies that tohdite was stabilized in a nanosize regime analogous to γ-Al_2O_3 having a lower surface energy and higher entropy due to cation occupancy in both the tetrahedral and octahedral sites. The domination of γ-Al_2O_3 at nanosize is due to its lower surface energy yet higher entropy than α-Al_2O_3.[26] (γ-Al_2O_3 has fair random distribution of Al^{3+} and vacancies over tetrahedral and octahedral sites in the spinel-type structure, whereas α-Al_2O_3 has all Al^{3+} in octahedral sites.[26]) Ti dopant may further increase the configurational energy of tohdite.

As for the corundum formation in the present system, it is apparently an epitaxial nucleation and growth process taking advantage of the catalytic effect of titania. In fact, the present rutile crystallized first as rods and geniculated twins, which then acted as heterogeneous nuclei[27] for the epitaxial nucle-

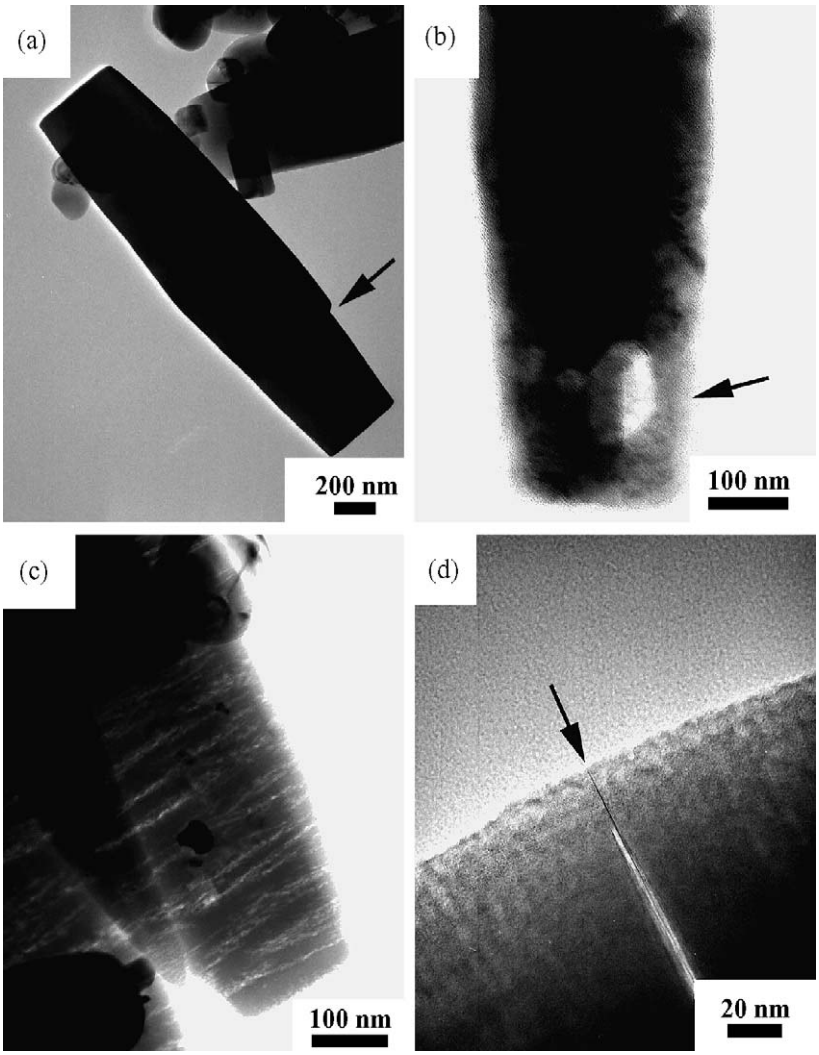

Fig. 6. TEM (BFI) for defect microstructures of tohdite in sample #1: (a) growth ledge (denoted by an arrow), (b) nanopores indicated by an arrow, (c) nano- to micro-cracks (light) and delaminated nanosheets (dark) parallel to the basal layers, (d) a large microcrack (arrow) formed by coalescence of the smaller ones parallel to the basal layer during electron irradiation for minutes.

ation of Ti-doped α-Al_2O_3. Rutile was indeed formed before α-Al_2O_3 upon short firing at 675 °C and 8.5 kbar, analogous to ambient pressure segregation of titania component from sol–gel Al_2O_3–TiO_2 mixed oxides to form rutile nuclei which induces further formation of α-Al_2O_3 at high temperature.[14]

4.2. Transient phases at specific T–P path

Fig. 9 is a tentative time–temperature-transformation (TTT) diagram showing the evolution of alumina hydrate/alumina phase assemblages observed at specified pressures and temperatures. The onset devitrification of hydrous sol–gel Al_2O_3–TiO_2 at relatively low temperature and pressure (∼500 °C and 1.5 kbar) caused the formation of χ-Al_2O_3, tohdite, nordstrandite, boehmite, and titania in the form of anatase and rutile (Table 1). Tohdite appeared to form at the expense of more hydrated species upon further dwelling under such a low grade *T–P* condition. A higher *T–P* path (above ca. 675 °C and 8 kbar) caused direct formation of less hydrated alumina species, i.e. tohdite and nordstrandite in the incipient devitrification stage and β-Al_2O_3 and α-Al_2O_3 after a longer dwelling time (cf. Fig. 9 and Table 1).

The evolution of transient alumina hydrate/alumina phases was little affected by the presence of additional water except at relatively low temperature and pressure (cf. Table 1). The observed transformation route is consistent with the reported sequence.[4,6,7] Tohdite, in particular, has been suggested by Yamaguchi and others.[4,6] as an intermediate phase of corundum for the system Al_2O_3·H_2O. Okumiya et al.,[7] showed further that tohdite dehydrated as α-Al_2O_3via intermediate κ′-Al_2O_3 and then κ-Al_2O_3. Tohdite could also be an independent phase of corundum because they are not found to associate with each other epitaxially in the present study.

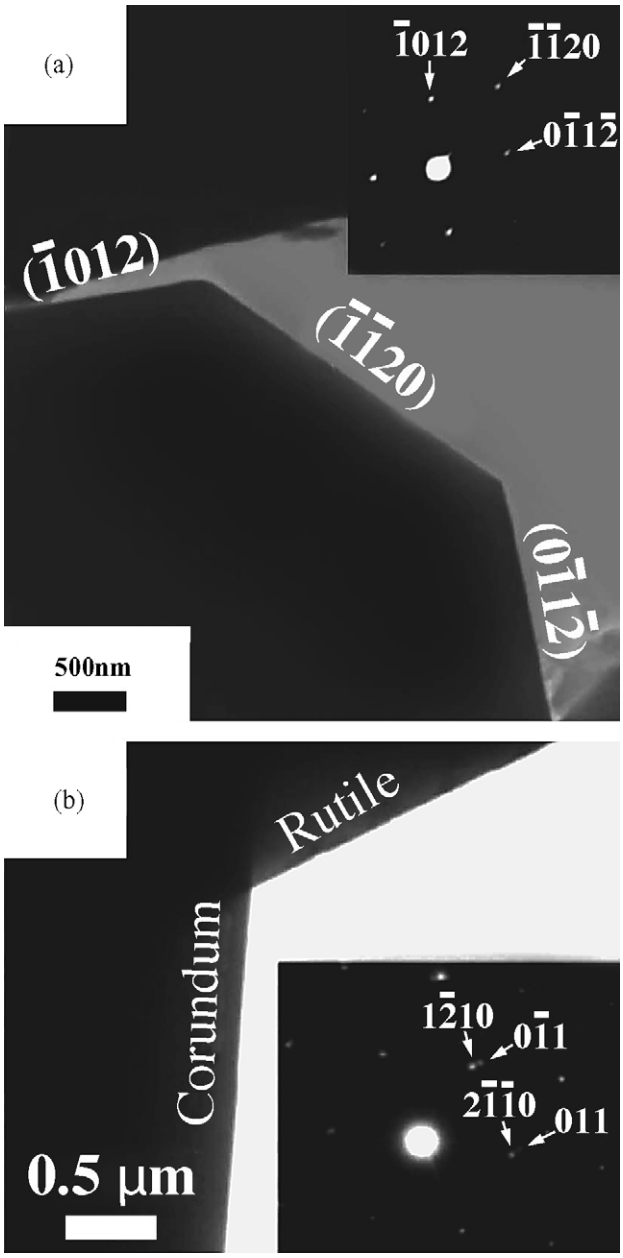

Fig. 7. TEM BFI and inset SAED pattern of (a) typical hexagonal-rhombohedral corundum in [2 $\bar{2}$ 0 1] zone axis with well-developed ($\bar{1}$ 0 1 2), ($\bar{1}$ $\bar{1}$ 2 0), and (0 $\bar{1}$ 1 $\bar{2}$) faces edge-on, in sample #3, and (b) epitaxial rutile and corundum in [0 0 1] and [0 0 0 1] zone axis, respectively in sample #4.

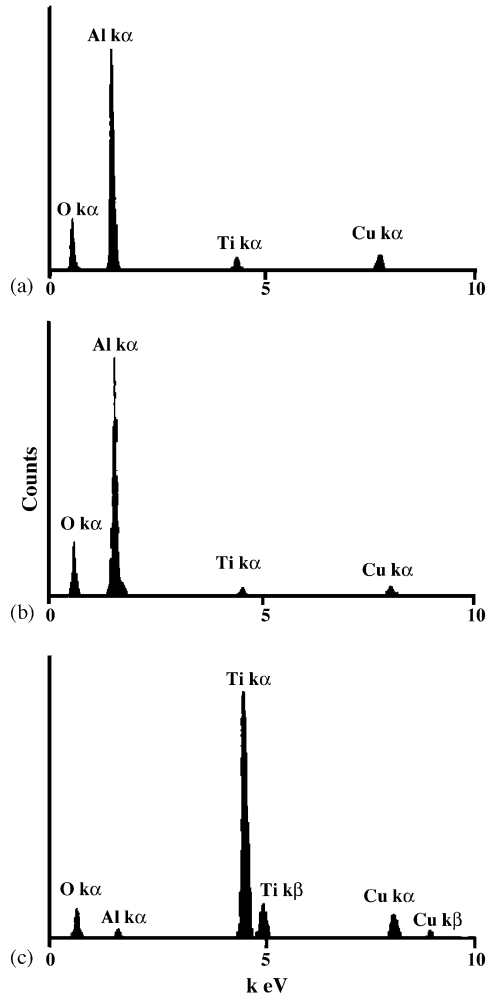

Fig. 8. Point count EDX spectrum of (a) tohdite with 3 at.% Ti in sample #2. (b) corundum dissolved with 2 at.% Ti in sample #3, and (c) rutile with 2 at.% Al in sample #5.

4.3. Superstructure and defects of Ti-doped tohdite

The present hydrous sol–gel Al_2O_3–TiO_2 fired at various *T–P* conditions showed decomposition defect microstructures for tohdite but not corundum despite nearly the same dopant level of Ti and common hexagonal symmetry with close-packed oxygen ion layers. This is due to significant amounts of H_2O in the former but not the latter. In fact, infrared absorption spectra indicated the presence of water molecules with characteristic band at 3269 cm^{-1} for tohdite. A higher frequency for OH stretching, yet lower frequency for OH deformation in the present sample, can be attributed to Ti content as mentioned. There are two types of aluminum positions for tohdite, i.e. four-fifths in octahedral and the rest in tetrahedral sites.[3] The ionic radii of Ti^{4+} and Al^{3+} are 0.0605 and 0.0535 nm, respectively, in coordination number (CN) 6, and 0.042 and 0.039 nm, respectively, in CN 4.[29] The superstructure and defect microstructures of Ti-doped tohdite may be caused by the substitution and ordering of Ti^{4+} with Al^{3+} in coordination number 6 and/or 4 with Al vacancies as charge and volume compensation defects. The substitution scheme is that three Ti^{4+} ions substitute for four Al^{3+} ions and leave one Al site vacant according to the following equation and the defect notation of Kröger and Vink[30]:

$$3TiO_2 \xrightarrow{Al_2O_3} 3Ti_{Al}^{\bullet} + V_{Al}''' + 6O_O^x$$

As the aluminium vacancy is triply charged, the site fractions of defects produced are related by[12]:

$$[V_{Al}'''] = 1/3[Ti_{Al}^{\bullet}]$$

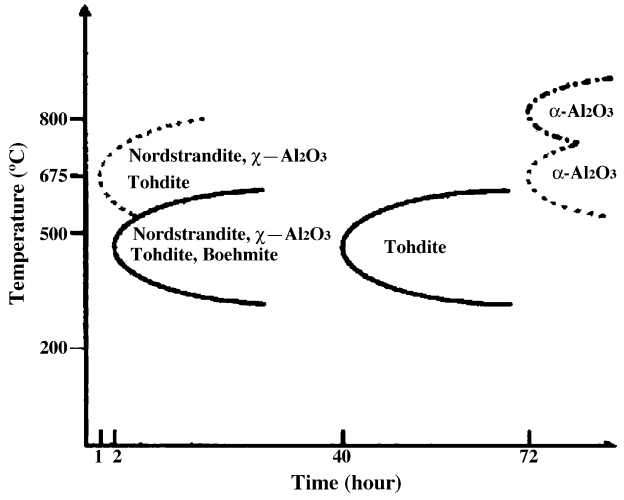

Fig. 9. A tentative and simplified TTT diagram showing alumina hydrates and alumina polymorphs were developed sequentially from hydrous Al_2O_3–TiO_2 gel when fired at specified pressures and temperatures without additional water. Solid, dotted and dot-dashed lines denote the TTT boundaries based on the present experimental results of 1.5 kbar, 500 °C; 8.5 kbar, 675 °C; and 9.0 kbar, 800 °C, respectively.

Given the cation dimensions and charges, it is clear that the Ti doping has to change the vacancy or interstitial defect concentration, but these defects are likely to be ordered in the lattice. The point defect distribution, whether it is random or orderly, should have a large effect on the diffusion and transformation rate of Ti-doped tohdite upon dehydration.

Decomposition of tohdite was previously studied using differential thermal analysis and thermogravimetric measurements[7] and electron irradiation.[31] The present electron irradiation in addition showed the formation of microcracks in accompaniment with the decomposition. The microcracks were observed to coalesce significantly to form large cracks parallel to the basal layer upon electron irradiation for minutes. This crack-coalescence behavior is analogous to electron-irradiation induced dehydroxylation of interstratified phyllosilicates under the influence of capillarity effect and shear stress with accompanying faulting and shuffling of basal layers.[20] It is an open question whether or not the formation of pores and microcracks parallel to the basal layers of tohdite were due to specific water/hydroxy ion occupancy or aluminium vacancy clusters in the basal layers, besides the electron bombardment effect. In any case, microcracks were affected by anisotropic volume shrinkage involved in the transformation of tohdite to more stable alumina. (The densities of all the transition aluminas are appreciably lower than that of corundum, so that significant volume shrinkage is involved in any transformation to corundum. Moreover this volume change is significantly anisotropic.)

4.4. Industrial and geological implications of Ti-doped tohdite and α-Al_2O_3

No commercial use of tohdite has been reported in the Science technology handbook for alumina.[13] The present Ti-doped tohdite and alumina with specific microstructures may have potential engineering applications. Ti ion termination in basal layers or ledged lateral surfaces and nano to mesosize pores in coalescence along the basal layer are expected to affect the catalytic properties of activated alumina, i.e. porous alumina which were extensively used as an industrial adsorbent, catalyst, and catalyst support.[32,33] The delaminated alumina sheets of nanometer thickness would provide large surface areas as alumina nanofibers fabricated from aluminum hydrates in the presence of poly(ethylene oxide) surfactant.[34] Ti-doped α-Al_2O_3 is also important to gem business and industrial applications.

As for geological implications, Ti-bearing tohdite was recently found as inclusion in garnet from whiteschist of the Kokchetav ultrahigh-pressure terrane, Kazakhstan[9] and metamorphosed paleosols in the Tananao metamorphic complex of Taiwan (Hwang et al., in preparation). In the former case, tohdite co-exists with quartz and rutile as inclusions in garnet. The peak metamorphic *P–T* condition of the whiteschist was estimated to be 720–760 °C and 34–36 kbar.[35] In the latter case, tohdite co-exists with rutile, quartz and zircon in garnet. The peak metamorphic condition for the paleosols was 660–690 °C and 8.3–8.8 kbar.[36] The present HTHP experimental results of hydrous TiO_2–Al_2O_3 gel showed that tohdite can be synthesized as a transient phase in the latter *T–P* range and a higher temperature led to α-Al_2O_3. Tohdite, in both natural occurrences, is therefore more like a retrograde phase, and was probably formed in a water-deficient micro-environment during rock exhumation.

5. Conclusions

1. Ti-doped α-Al_2O_3 was synthesized from sol–gel Al_2O_3–TiO_2 at relatively high *T–P* conditions (above 675 °C at ca. 8 kbar), and optimum *T–P* conditions (e.g. 500 °C and 1.5 kbar) favored tohdite formation. The sol–gel remained amorphous when fired below 675 °C at ambient pressure. Additional water affects little the phase assemblages except in the incipient devitrification stage at lower *P–T* conditions.
2. Ti-doped tohdite crystals are elongated along the crystallographic *c*-axis with well-developed (0 0 0 1) base and a full set of ledges $\{1\,0\,\bar{1}\,0\}$. A significant water/hydroxy ion content, the substitution of Ti^{4+} and Al^{3+} in tetrahedral and/or octahedral sites with charge compensating Al vacancies, and electron dosage account for the superstructures and defect microstructures of the tohdite lattice.
3. The formation of Ti-doped tohdite and α-Al_2O_3 was catalyzed by Ti^{4+} coordination effect and epitaxial rutile nuclei, respectively.
4. The status report on the stability of Ti-doped alumina hydrate and alumina phases sheds light on the natural genesis of tohdite from paleosols and peraluminous metamorphic rocks.

Acknowledgments

We thank Miss C.H Su for her technical assistance on FTIR, Mr. Jacob Chu for reading the manuscript and an anonymous referee for constructive comments. This research was supported by Center for Nanoscience and Nanotechnology at NSYSU.

Appendix A

(a) and (b) are, respectively, the top view of the unrelaxed (0 0 0 1) and $\{1\,0\,\bar{1}\,0\}$ faces of tohdite with crystallographic directions specified. Large gray circles, medium light gray circles and small dark circles denote O, Al and H atoms, respectively. A tohdite unit-cell contains four closely packed yet distorted oxygen layers stacked in ABAC sequence along the *c*-axis (Yamaguchi et al.[37]). There are total 10 Al atoms in the unit cell, two at (2/3, 1/3, ∼1/8) equivalent positions in octahedral sites, six at equivalent (∼1/6, ∼1/3, ∼3/8) positions in octahedral sites, and two at (1/3, 2/3, ∼1/16) equivalent positions in tetrahedral sites.

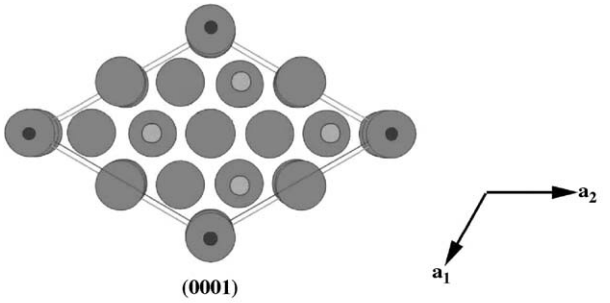

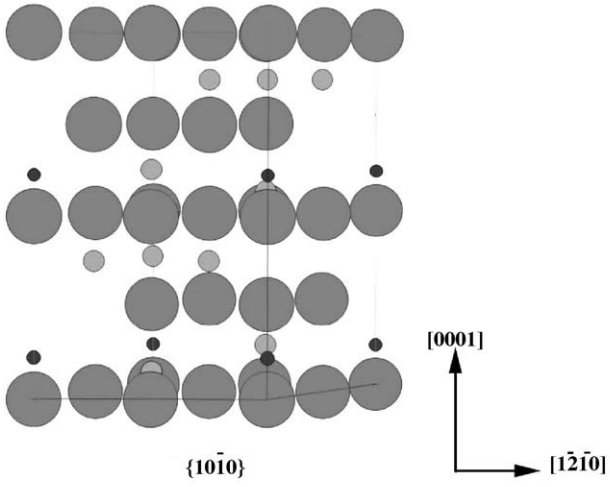

References

1. Levin, I. and Brandon, D., Metastable alumina polymorphs: crystal structures and transition sequences. *J. Am. Ceram. Soc.*, 1998, **81**(8), 1995–2012.
2. Digne, M., Sautet, P., Raybaud, P., Toulhoat, H. and Artacho, E., Structure and stability of aluminum hydroxides: a theoretical study. *J. Phys. Chem. B*, 2002, **106**, 5155–5162.
3. Yamaguchi, G., Yanagida, H. and Ono, S., The crystal structure of tohdite. *Bull. Chem. Soc. Jpn.*, 1964, **37**, 1555–1557.
4. Yamaguchi, G., Yanagida, H. and Ono, S., A new alumina hydrate, "tohdite" ($5Al_2O_3{\cdot}H_2O$). *Bull. Chem. Soc. Jpn.*, 1963, **37**, 752–754.
5. Yamaguchi, G., Yanagida, H., Ono, S., Miki, T. and Seto, A., Three new synthetic minerals with tohdite-like structures. *Bull. Chem. Soc. Jpn.*, 1965, **38**, 1226.
6. Yamaguchi, G., Yanagida, H. and Ono, S., Condition of tohdite $5Al_2O_3{\cdot}H_2O$ formation. *J. Ceram. Assoc. Jpn.*, 1966, **74**, 84–88.
7. Okumiya, M., Yamaguchi, G., Yamada, O. and Ono, S., The formation of k- and k′-Al_2O_3 from the dehydration if tohdite $5Al_2O_3{\cdot}H_2O$. *Bull. Chem. Soc. Jpn.*, 1971, **44**, 418–423.
8. Guzmán-Mendoza, J., García-Hipólito, M., Aguilar-Frutis, M. and Falcony-Guajardo, C., Structure characteristics of Al_2O_3 thin films prepared by spray pyrolysis. *J. Phys. Condens. Matter*, 2001, **13**(50), L955–L959.
9. Hwang, S. L., Yui, T. F., Chu, H. T., Shen, P., Liou, J. G., Sobolev, N. V., Zayachkovsky, A. A., *Tohdite: a new alumina hydrate phase from whiteschist of the Kokchetav ultrahigh-pressure terrane, Kazakhstan*. CNMMN (IMA No. 2004-051), 2005, personal communication.
10. Sugiyama, A., Fukuyama, H., Sasuga, T., Arisawa, T. and Takuma, H., Direct bonding of Ti:sapphire laser crystals. *Appl. Optics*, 1998, **37**(12), 20.
11. Wang, T. H., Zhao, Y. C., Wang, M. Z. and Zang, J. B., Structure and properties of diamond grits coated with corundum micron powders. *Key Eng. Mater.*, 2003, **250**, 94–98.
12. Phillips, D. S., Heuer, A. H. and Mitchell, T. E., Precipitation in star sapphire. I. Identification of the precipitate. *Philos. Magazine A*, 1980, **42**(3), 385–404.
13. Hart, L. D. and Lense, E., *Alumina Chemicals: Science and Technology Handbook*. American Ceramic Society, Westerville, Ohio, 1990, p. 15.
14. Montoya, J. A., Angel, P. D. and Viveros, T., The effect of temperature on the structural and textural evolution of sol–gel Al_2O_3–TiO_2 mixed oxides. *J. Mater. Chem.*, 2001, **11**, 944–950.
15. Williams, D. B., *Practical Analytical Electron Microscopy in Materials Science*. Philips Electronic Instruments Inc, Mahwah, 1984.
16. Wang, S. L., Johnston, C. T., Bish, D. L., White, J. L. and Hem, S. L., Water–vapor adsorption and surface area measurement of poorly crystalline boehmite. *J. Colloid Interface Sci.*, 2003, **260**, 26–35.
17. Yunxia, J., Guanghai, L., Yong, Z., Yunxia, Z. and Lide, Z., Photoluminescence of anatase TiO_2 thin films achieved by the addition of $ZnFe_2O_4$. *J. Phys. Condens. Matter*, 2001, **13**, L913–L918.
18. Liu, P. and Skogsmo, J., Space-group determination and structure model of κ-Al_2O_3 by Convergent-beam electron diffraction (CBED). *Acta Cryst. B*, 1991, **47**, 425–433.
19. Yourdshahyan, Y., Ruberto, C., Halvarsson, M., Bengtsson, L., Langer, V. and Lundqvist, B. I., Theoretical structure determination of a complex materials: κ-Al_2O_3. *J. Am. Ceram. Soc.*, 1999, **82**(6), 1365–1380.
20. Shen, P., Hwang, S. L. and Chu, H. T., Defect microstructure and dehydroxylation mechanism of interstratified phyllosilicates: a TEM study. *J. Mater. Sci.*, 1990, **25**, 3072–3078.
21. Kogure, T., Dehydration sequence of gibbsite by electron-beam irradiation in a TEM. *J. Am. Ceram. Soc.*, 1999, **82**(3), 716–720.
22. Porter, D. A. and Easterling, K. E., *Phase Transformations in Metals and Alloys*. Chapman & Hall, UK, 1992.
23. McMillan, P. W., *Glass Ceramics* (*2nd ed.*). Academic Press, London, 1979, p. 76.
24. Mysen, B. O., Structure and properties of silicate melts. *Development in Geochemistry* (*4th ed.*). Elsevier, Amsterdam, 1988, p. 187.
25. Lin, C. C. and Shen, P., The role of Ti^{4+} on the structure and transformations of gel-produced Zn_2SiO_4. *J. Solid State Chem.*, 1994, **112**, 381–386.

26. McHale, J. M., Auroux, A., Perrotta, A. J. and Navrotsky, A., Surface energies and thermodynamic phase stability in nanocrystalline aluminas. *Science*, 1997, **277**, 788–791.
27. Bond, G. C., *Heterogeneous Catalysis: Principles and Applications* (*2nd ed.*). Clarendon Press, Oxford, 1990, pp. 176.
28. Mathieu, D., Philippe, S., Pascal, R., Hervé, T. and Emilio, A., Structure and stability of aluminum hydroxides: a theoretical study. *J. Phys. Chem. B*, 2002, **106**, 5155–5162.
29. Shannon, R. D., Revised effective ionic radii and systematic studies of interatomic distances in halides and chalcogenides. *Acta Cryst. A*, 1976, **32**, 751–767.
30. Kröger, F. A. and Vink, H. J., Relations between the concentrations of imperfections in crystalline solids. *Solid State Phys.*, 1956, **3**, 307–435.
31. Krischner, V. H., Electron diffraction investigation on Al_2O_3-KI. *Ber. Deut. Keran. Ges.*, 1966, **43**, 479–483.
32. Goodboy, K. P. and Dowing, K. C., In *In Alumina Chemicals: Science and Technology Handbook*, ed. L. D. Hart and E. Lense. The American Ceramic Society Inc., Westerville, OH, 1990, p. 93.
33. Trim, D. L. and Stanislaus, A., The control of pore size in alumina catalyst supports: a review. *Appl. Catal.*, 1986, **21**, 215–238.
34. Zhu, H. Y., Riches, J. D. and Barry, J. C., Alumina nanofibers prepared from aluminum hydrate with poly(ethylene oxide) surfactant. *Chem. Mater.*, 2002, **14**(4), 2086–2093.
35. Parkinson, C. D., Coesite inclusions and prograde compositional zonation of garnet in whiteschist of the HP-UHPN Kokchetav massif, Kazakhstan: a record of progressive UHP metamorphism. *Lithos*, 2000, **52**, 215–233.
36. Hwang, S. L., Yui, T. F., Chu, H. T. and Shen, P., Submicron polyphase inclusions in garnet from the Tananao Metamorphic Complex, Taiwan: a key to unraveling otherwise unrecognized metamorphic events. *J. Metamorphic Geol.*, 2001, **19**, 599–605.
37. Yamaguchi, G., Okumiya, M. and Ono, S., Refinement of the structure of tohdite $5Al_2O_3{\cdot}H_2O$. *Bull. Ceram. Soc. Jpn.*, 1969, **42**, 2247–2249.